Available online at www.sciencedirect.com
ScienceDirect
Construction and Building Materials 21 (2007) 1052–1060
Construction and Building MATERIALS
www.elsevier.com/locate/conbuildmat

An approach to determine long-term behavior of concrete members prestressed with FRP tendons

Samer A. Youakim, Vistasp M. Karbhari *

Department of Structural Engineering, MC-0085, University of California, San Diego, La Jolla, CA 92093-0085, USA

Received 8 August 2005; received in revised form 23 January 2006; accepted 6 February 2006
Available online 6 May 2006

Abstract

The combined effects of creep and shrinkage of concrete and relaxation of prestressing tendons cause gradual changes in the stresses in both concrete and prestressing tendons. A simple method is presented to calculate the long-term prestress loss and the long-term change in concrete stresses in continuous prestressed concrete members with either carbon fiber reinforced polymer (CFRP) or aramid fiber reinforced polymer (AFRP) tendons. The method satisfies the requirements of equilibrium and compatibility and avoids the use of any empirical multipliers. A simple graph is proposed to evaluate the reduced relaxation in AFRP tendons. It is shown that the prestress loss in FRP tendons is significantly less than that when using prestressing steel, mainly because of the lower moduli of elasticity of FRP tendons. The long-term changes in concrete stresses and deflection can be either smaller or greater than those of comparable girders prestressed with steel tendons, depending on the type of FRP tendons and the initial stress profile of the cross-section under consideration.

Keywords: Creep; FRP; Long-term; Prestress loss; Prestressed concrete; Relaxation; Shrinkage

1. Introduction

The use of fiber reinforced polymer (FRP) tendons as prestressing reinforcements have been proposed in the past decade and a few concrete bridges have already been constructed utilizing fiber reinforced polymer (FRP) tendons. Compared to conventional steel prestressing tendons, FRP tendons have many advantages, including their noncorrosive and nonconductive properties, lightweight, and high tensile strength. Most of the research conducted on concrete girders prestressed with FRP tendons has focused on the short-term behavior of prestressed members; research findings on the long-term behavior of concrete members with FRP tendons are scarce in the literature. The recent ACI Committee report on prestressing concrete structures with FRP tendons (ACI 440.4R-04 [1]) has pointed out that: "Research on the long-term loss of prestress and the resultant time-dependent camber/deflection is needed ..." Most of the research and applications of FRP tendons in concrete structures have adopted either carbon fiber reinforced polymer (CFRP) or aramid fiber reinforced polymer (AFRP) tendons. The use of glass fiber reinforced polymers (GFRP) has mostly been limited to conventional reinforcing bars due to their relatively low tensile strength and poor resistance to creep. Therefore, this paper focuses on prestressed members with either CFRP or AFRP tendons.

Creep and shrinkage of concrete, and relaxation of prestressing tendons, cause long-term deformations in concrete structures. While it is generally accepted that long-term losses do not affect the ultimate capacity of a prestressed concrete member, a reasonably accurate prediction of these losses is important to ensure satisfactory performance of concrete structures in service. If prestress losses are underestimated, the tensile strength of concrete can be exceeded under full service loads, causing cracking and unexpected excessive deflection. On the other hand, overestimating

* Corresponding author. Tel.: +1 858 534 6470; fax: +1 858 534 6373.
E-mail address: vkarbhari@ucsd.edu (V.M. Karbhari).

0950-0618/$ - see front matter © 2006 Elsevier Ltd. All rights reserved.
doi:10.1016/j.conbuildmat.2006.02.006

Nomenclature

A	area of cross section
d	vertical distance measured from top fiber of cross section
E	modulus of elasticity
$\overline{E}_c(t,t_0)$	age-adjusted elasticity modulus of concrete
f_{pu}	ultimate strength of prestressing tendon
h	total thickness of concrete cross section
I	second moment of area
O	centroid of age-adjusted transformed section
t	final time (end of service life of concrete member)
t_0	concrete age at prestressing
y	coordinate of any fiber measured downward from O
χ	aging coefficient
χ_r	reduced relaxation coefficient
α	ratio of modulus of elasticity of FRP or steel to that of concrete
$\Delta\varepsilon_c(t,t_0)$	change in concrete strain between time t_0 and t
$\Delta\varepsilon_O$	change in axial strain at the centroid of age-adjusted transformed section O
$\Delta\sigma_c(t,t_0)$	stress applied gradually from time t_0 to its full amount at time t
$\Delta\sigma_{pr}$	intrinsic relaxation
$\Delta\bar{\sigma}_{pr}$	reduced relaxation
$\Delta\sigma_p$	total long-term prestress loss
$\Delta\psi$	change in curvature
ε_{cs}	shrinkage strain of concrete between t_0 and t
$\varepsilon_c(t_0)$	instantaneous strain at time t_0
$\varphi(t,t_0)$	creep coefficient between t_0 and t
$\sigma_c(t_0)$	stress applied at time t_0 and sustained to a later time t
σ_{p0}	initial stress of prestressing tendon
ρ	reinforcement ratio
ψ	curvature
Ω	the ratio of the difference between the total prestress loss and intrinsic relaxation to the initial stress

Subscripts

1	transformed section at t_0
c	concrete
cc	net concrete section
f	FRP reinforcement or flange
p	prestressing FRP tendon
ps	prestressing steel tendon
s	steel reinforcement

prestress losses can lead to excessive camber and uneconomic design.

The error in predicting the long-term prestress losses can be due to: (1) inaccuracy in estimation of the long-term material characteristics (creep and shrinkage of concrete and relaxation of prestressing tendons); and (2) inaccuracy of the method of analysis used. The objective of this paper is to address the second source of inaccuracy by presenting a simple analytical method to estimate the time-dependent strains and stresses in concrete members prestressed with FRP tendons. The method satisfies the requirements of equilibrium and compatibility and avoids the use of empirical equations, which in general show loss in accuracy to enable generality. The inaccuracy in the material characteristics used can be mitigated by varying the input material parameters and establishing upper and lower bounds on the analysis results.

For the purpose of this paper, and to avoid confusion, a consistent sign convention is used. Axial force N is positive when it is tensile. Bending moment, M, that produces tension at the bottom fiber of a cross section and the associated curvature ψ are positive. Stress, σ, and strain, ε, are positive for tension and elongation, respectively. Downward deflection is positive. It follows that shrinkage, ε_{cs}, is negative quantity. The loss in tension in prestressing reinforcement due to relaxation $\Delta\sigma_{pr}$ or due to the combined effects of creep, shrinkage, and relaxation, $\Delta\sigma_p$, is negative quantity. The analysis considered herein focuses on a prestressed concrete section with its centroidal principal y-axis in vertical direction with the coordinate y of any concrete fiber or steel layer being measured downward from a given reference point.

2. Relaxation of FRP prestressing tendons

Similar to concrete and steel, AFRP prestressing tendons exhibit some creep if subjected to sustained strains. CFRP tendons typically display insignificant amount of creep, which can be neglected for most practical applications. When a prestressing tendon is stretched between two points, it will be subjected to a constant strain. Because of creep, the stress in the tendon decreases (or relaxes) with time to maintain the state of constant strain. This reduction in stress is known as *intrinsic relaxation* $\Delta\sigma_{pr}$. While steel tendons subjected to stresses less than 50% of the yield stress do not exhibit appreciable amount of relaxation, tests on AFRP tendons have shown that they display relaxation under very low stresses. The level of relaxation of AFRP tendons depends upon many factors, including ambient temperature, environment (e.g., air, alkaline, acidic, or salt solutions), ratio of initial stress, σ_{p0}, to its ultimate strength, f_{pu}, and time t lapsed after initial stressing. Based on extensive experimentation on relaxation properties of AFRP tendons, Saadatmanesh and Tannous [2] suggested a relationship of the form:

$$\frac{\Delta\sigma_{pr}}{f_{pu}} = \frac{\lambda - (a - b\log t)}{\lambda} \tag{1}$$

where $\lambda = \sigma_{p1}/f_{pu}$. σ_{p1} is the stress in the tendon 1 h after stress release. Ratios of σ_{p1}/σ_{p0} in their tests varied between 0.91 and 0.96, with an average of 0.93. Tabulated values of the variables a and b were provided for $\lambda = 0.4$ and $\lambda = 0.6$, and for different temperature levels and solution types. For AFRP tendons in air at a temperature of 25 °C, relationships for a and b were proposed [2] as

$$a = \lambda - 0.03; \quad b = \frac{\lambda - 0.27}{23} \tag{2}$$

In a prestressed concrete member, the two ends of the prestressing tendon constantly move toward each other because of creep and shrinkage of concrete, thereby reducing the tensile stress in the tendon. This reduction in tension has a similar effect to that when the tendon is subjected to a lesser initial stress. Thus, a reduced relaxation value, $\Delta\bar{\sigma}_{pr}$, should be used in the analysis of long-term effects in prestressed members, such that

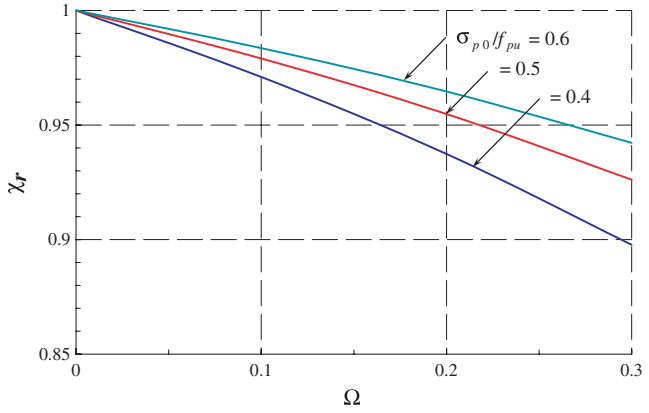

Fig. 1. Reduced relaxation coefficient χ_r for AFRP.

$$\Delta\bar{\sigma}_{pr} = \chi_r \Delta\sigma_{pr} \tag{3}$$

where χ_r is a dimensionless coefficient less than unity. Following an approach previously suggested by Ghali and Trevino [3] to evaluate χ_r for prestressing steel tendons, χ_r for AFRP tendons can be calculated as (log t in Eq. (1) is taken equal to 5 for 100,000 h):

$$\chi_r = \int_0^1 \frac{\lambda(1 - \Omega\zeta) - (a' - 5b')}{(1 - \Omega\zeta)(\lambda - (a - 5b))} \mathrm{d}\zeta \tag{4}$$

where

$$a' = \lambda(1 - \Omega\zeta) - 0.03; \quad b' = \frac{\lambda(1 - \Omega\zeta) - 0.27}{23} \tag{5}$$

and ζ is a dimensionless time function defining the shape of the tendon stress–time curve. The value of ζ increases from 0 to 1 as time changes from initial prestress time t_0 to final time t. Ω is the ratio of the difference between the total prestress loss $\Delta\sigma_{ps}(t)$ and intrinsic relaxation $\Delta\sigma_{pr}(t)$ to the initial stress σ_{p0}, expressed as

$$\Omega = -\frac{\Delta\sigma_{ps}(t) - \Delta\sigma_{pr}(t)}{\sigma_{p0}} \tag{6}$$

Fig. 1 shows the variation of χ_r with Ω for $\sigma_{p0}/f_{pu} = 0.4$, 0.5, and 0.6, which represents the common values of initial prestressing ratios [1]. As will be shown in a later section, Ω typically varies between 0.1 and 0.2 and a value of $\chi_r = 0.95$ can be assumed for practical purposes.

3. Proposed method of analysis

The analysis follows the four generic steps proposed by Ghali et al. [4] and depicted schematically in Fig. 2. The procedure can be developed considering an arbitrary

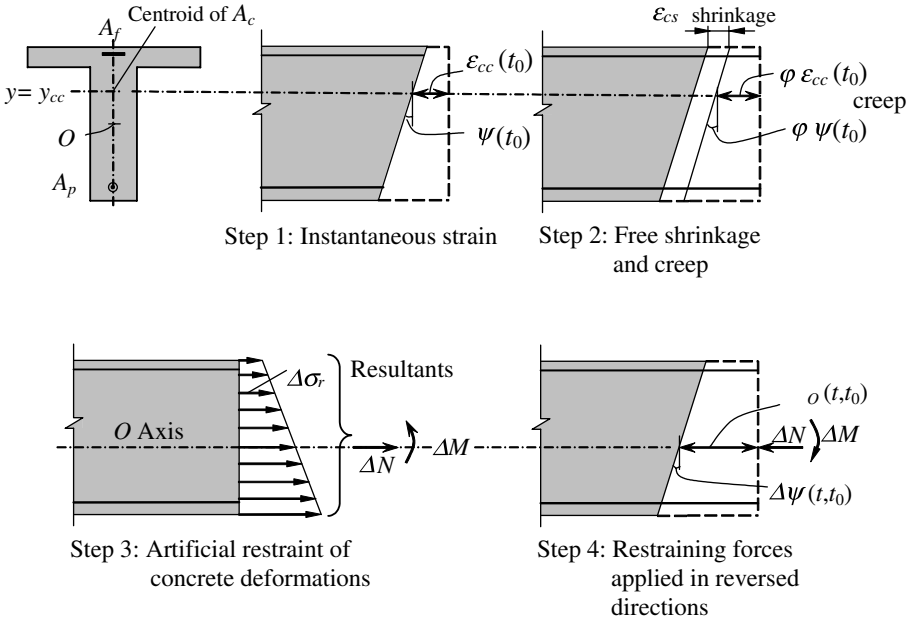

Fig. 2. Four steps of analysis of time-dependent effects (after Ghali et al. [4]).

section consisting of a simple type of concrete, subjected at time t_0 to both prestressing and dead loads. The method will result in a simple equation that is easy to use by practicing engineers instead of lengthy matrix analysis that could only be used in special-purpose computer programs. In addition to the initial strain profile of the cross section, the equation is only a function of four dimensionless coefficients that can be easily calculated (or interpolated from graphs) and the creep coefficient and shrinkage.

3.1. Initial steps

Step 1: *Instantaneous strains.* At any fiber, the strain and the curvature at time t_0 due to the dead load and prestressing effects (primary + secondary) can be calculated. Alternatively, at this stage, the designer may have determined the stress distribution at t_0 to verify that the allowable stresses are not exceeded. In this case, the strain diagram at t_0 can be obtained by dividing the stress values by the modulus of elasticity of concrete at t_0, $E_c(t_0)$.

Step 2: *Free creep and shrinkage of concrete.* The distribution of hypothetical free change in concrete strain due to creep and shrinkage in the period t_0 to t is defined by its value $(\Delta\varepsilon_{cc})_{free}$ at the centroid of the area of the net concrete section, A_c (defined as the gross area minus the area of the FRP reinforcement, A_f, minus the area of the prestressing duct in the case of post-tensioning, or minus the area of the FRP tendons, A_p, in case of pretensioning) at $y = y_{cc}$ as shown in Fig. 3, such that

$$(\Delta\varepsilon_{cc})_{free} = \varphi\varepsilon_{cc}(t_0) + \varepsilon_{cs} \tag{7}$$

where y_{cc} is the y coordinate of the centroid of the net concrete section, φ is the creep coefficient for the period t_0 to t, and ε_{cs} is the shrinkage in the same period and $\varepsilon_{cc}(t_0)$ is the strain at the centroid of the net concrete section given by

$$\varepsilon_{cc}(t_0) = \varepsilon_1(t_0) + (y_{cc} - y_1)\psi(t_0) \tag{8}$$

where y_1 is the centroid of the transformed area at t_0, and $\psi(t_0)$ is the curvature (slope of the strain diagram) at t_0. Also free curvature is

$$\Delta\psi_{free} = \varphi\psi(t_0) \tag{9}$$

Step 3: *Artificial restraining forces.* The free strain calculated in Step 2 can be artificially prevented by a gradual application of restraining stress, whose value at any fiber y is given by

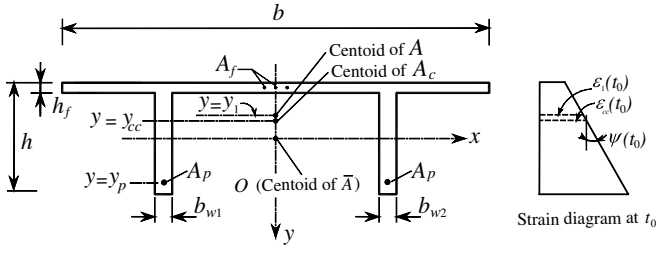

Fig. 3. Typical prestressed concrete section and the strain diagram immediately after transfer.

$$\sigma_r = -\overline{E}_c[(\Delta\varepsilon_{cc})_{free} + \Delta\psi_{free}y] \tag{10}$$

where $\overline{E}_c$ is the age-adjusted modulus of concrete [5,6], used to account for creep effects of stresses applied gradually to concrete and is defined as

$$\overline{E}_c = \frac{E_c(t_0)}{1 + \chi\varphi} \tag{11}$$

The artificial restraining forces, ΔN at the reference point O (which is the centroid of the age-adjusted transformed section), and ΔM, that can prevent strain changes due to creep, shrinkage and relaxation can be defined as

$$\Delta N = -\overline{E}_c A_c(\Delta\varepsilon_{cc})_{free} + A_p\Delta\bar{\sigma}_{pr} \tag{12}$$

and

$$\Delta M = -\overline{E}_c I_c\Delta\psi_{free} - \overline{E}_c A_c(\Delta\varepsilon_{cc})_{free}y_{cc} + y_p A_p\Delta\bar{\sigma}_{pr} \tag{13}$$

where I_c, y_p, and $\Delta\bar{\sigma}_{pr}$ are the second moment of A_c about its centroid, y coordinate of the centroid of the FRP tendons, and the reduced relaxation stress between times t_0 and t. It should be noted that if the section contains more than one layer of prestresssing tendons, the terms containing A_p or y_pA_p should be substituted by the sum of the appropriate parameters for all layers.

Step 4: *Elimination of artificial restraint.* The artificial forces ΔN and ΔM can be applied in reversed direction on the age-adjusted transformed section to give the true change in strain at O, $\Delta\varepsilon_O$, and in curvature, $\Delta\psi$, such that

$$\Delta\varepsilon_O = -\Delta N/(\overline{E}_c\overline{A}) \tag{14a}$$

$$\Delta\psi = -\Delta M/(\overline{E}_c\overline{I}) \tag{14b}$$

where $\overline{I}$ is the second moment of $\overline{A}$ about its centroid and $\overline{A}$ is the area of age-adjusted transformed section defined as

$$\overline{A} = A_c + A_f\left(\frac{E_f}{\overline{E}_c}\right) + A_p\left(\frac{E_p}{\overline{E}_c}\right) \tag{15}$$

where E_f and E_p are the moduli of elasticity for the FRP reinforcement and tendons, respectively, and the $\overline{E}_c$ is as defined in Eq. (11).

Substituting Eqs. (12) and (13) into Eqs. (14) and (15) gives

$$\Delta\varepsilon_O = k_A(\Delta\varepsilon_{cc})_{free} - \frac{A_p}{\overline{A}}\frac{\Delta\bar{\sigma}_{pr}}{\overline{E}_c} \tag{16}$$

and

$$\Delta\psi = k_I\Delta\psi_{free} + \frac{k_{cc}}{h}(\Delta\varepsilon_{cc})_{free} - \frac{A_p y_p}{\overline{I}}\frac{\Delta\bar{\sigma}_{pr}}{\overline{E}_c} \tag{17}$$

where

$$k_A = \frac{A_c}{\overline{A}};\quad k_I = \frac{I_c}{\overline{I}};\quad k_{cc} = \frac{A_c y_{cc}h}{\overline{I}};$$

$$k_p = 1 - \frac{E_p}{\overline{E}_c}\left(\frac{A_p}{\overline{A}} + \frac{A_p y_p^2}{\overline{I}}\right) \tag{18}$$

The time-dependent change in strain in prestressing tendons $\Delta\varepsilon_p$ can then be evaluated using Eq. (19) and the

time-dependent change in stress in prestressing tendons (described by Eq. (20)) is the sum of $E_p\Delta\varepsilon_p$ and the reduced relaxation.

$$\Delta\varepsilon_p = \Delta\varepsilon_O + y_p\Delta\psi \tag{19}$$

$$\Delta\sigma_p = E_p(\Delta\varepsilon_O + y_p\Delta\psi) + \Delta\bar{\sigma}_{pr} \tag{20}$$

Substitution of Eqs. (16) and (17) into Eq. (20) gives an expression for the long-term prestress loss, $\Delta\sigma_p$, due to creep, shrinkage, and relaxation as

$$\Delta\sigma_p = E_p\left\{k_A(\Delta\varepsilon_{cc})_{free} + y_p\left[k_I\Delta\psi_{free} + \frac{k_{cc}(\Delta\varepsilon_{cc})_{free}}{h}\right]\right\} + k_p\Delta\bar{\sigma}_{pr} \tag{21}$$

It should be noted that the last term in Eq. (21), $k_p\Delta\bar{\sigma}_{pr}$, is zero in the case of prestressed members using CFRP tendons.

3.2. Time-dependent change in concrete stress

The time-dependent change in concrete stress at any fiber at distance y from O is the sum of the restraining stress (Eq. (10)) and the stress due to $-\Delta N$ and $-\Delta M$:

$$\Delta\sigma = \sigma_r + \overline{E}_c(\Delta\varepsilon_O + y\Delta\psi) \tag{22}$$

3.3. Long-term deflection

Inaccurate prediction of the change in deflection with time in concrete bridges can lead to problems with bridge grading or excessive deflection or camber. In residential buildings or parking structures, it might cause discomfort to occupants, or problems such as related to water ponding. The long-term deflection, ΔD, of a structural member of a plane frame can be calculated by numerical integration of the long-term change in curvatures, $\Delta\psi$ (Eq. (17)) at a number of equally spaced sections. Eqs. (23) and (24) give, respectively, ΔD at mid-span in terms of $\Delta\psi$ at 3 and 5 sections assuming parabolic variation of curvature between sections.

$$\Delta D = \frac{l^2}{96}(\Delta\psi_1 + 10\Delta\psi_2 + \Delta\psi_3) \tag{23}$$

$$\Delta D = \frac{l^2}{192}(\Delta\psi_1 + 6\Delta\psi_2 + 10\Delta\psi_3 + 6\Delta\psi_4 + \Delta\psi_5) \tag{24}$$

4. Application to continuous girders

Prestressing of continuous beams or frames produces statically indeterminate bending moments (referred to as secondary moments). As mentioned previously, $\varepsilon_1(t_0)$ and $\psi(t_0)$ (Eqs. (7)–(9)) represent the strain parameters at a section due to dead load plus the primary and secondary moments due to prestressing. The time-dependent change in prestress force in the tendon produces changes in these secondary moments, which are not included in Eq. (21). This section considers the effect of the time-dependent change in secondary moments on the prestress loss.

Step 1: Considering a two-span continuous beam, as shown in Fig. 4(a) where the variation of the tendon profile is parabolic in each span, the statically indeterminate beam can be solved by any method of structural analysis (such as the force method) to determine the moment diagram at time t_0 due to dead load and prestressing.

Step 2: The time-dependant sectional analysis can be performed as shown previously for each of the three sections shown in Fig. 4(b) and determine $(\Delta\psi)_i$ for each section, where $i = A$, B and C.

Step 3: Use the force method to determine the change in internal forces and displacements in the continuous beam. The released structure with the shown coordinate system in Fig. 5(a) can be used. It can be assumed that the change in angular discontinuity at middle support between t_0 and t is ΔD_1 and that the unknown change in the connecting moment is ΔF_1. The change in angular discontinuity ΔD_1 is then evaluated as the sum of the two end rotations of each of the simple spans l_1 and l_2. Using the method of elastic weights and assuming a parabolic variation of curvature in each span, ΔD_1 can be expressed as

$$\Delta D_1 = \frac{-l_1}{6}[2(\Delta\psi)_A + (\Delta\psi)_B] + \frac{l_2}{6}[2(\Delta\psi)_C + (\Delta\psi)_B] \tag{25}$$

Step 4: Due to unit load of the connecting moment $\Delta F_1 = 1$ that is to be applied gradually on the released structure from zero at time t_0 to unity at time t (Fig. 5(b)), determine the change in curvature at each section $(\Delta\psi_{u1})_i$ as

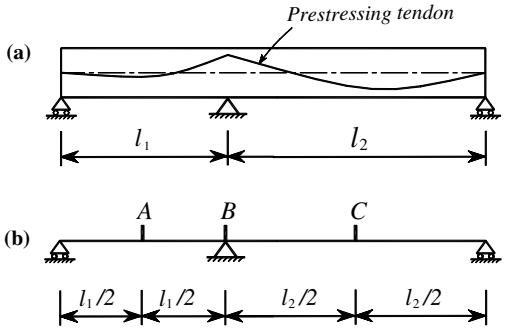

Fig. 4. Two-span continuous prestressed girder. (a) Dimensions and cable profile; (b) Locations of integration points (sections).

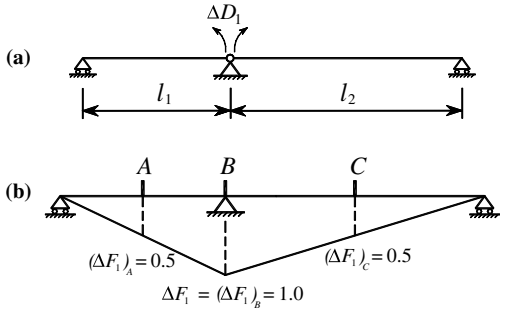

Fig. 5. Analysis by the force method. (a) Released structure and coordinate system; (b) Moment diagram due to unit value of connecting moment.

$$(\Delta\psi_{u1})_i = (\Delta F_1)_i/(\overline{E}_c\overline{I})_i \quad (26)$$

The age-adjusted flexibility coefficient $\overline{f}_{11}$ can be evaluated as

$$\overline{f}_{11} = \frac{l_1}{6}[2(\Delta\psi_{u1})_A + (\Delta\psi_{u1})_B] + \frac{l_2}{6}[(2(\Delta\psi_{u1})_C + (\Delta\psi_{u1})_B] \quad (27)$$

Step 5: The change in connecting moment ΔF_1 can be computed by solving the compatibility equation $\overline{f}_{11}\Delta F_1 + \Delta D_1 = 0$, i.e.,

$$\Delta F_1 = \frac{-\Delta D_1}{\overline{f}_{11}} \quad (28)$$

The prestress change (loss or gain) at each section due to continuity $(\Delta\sigma_{p(cont)})_i$ is then

$$(\Delta\sigma_{p(cont)})_i = \left(\frac{E_p}{\overline{E}_c}\right)\left(\frac{\Delta M}{\overline{I}}y_p\right)_i \quad (29)$$

where $(\Delta M)_i$ is the change in bending moment at each section. Thus, $(\Delta M)_A = (\Delta M)_B = \Delta F_1/2$ and $\Delta M_B = \Delta F_1$. Consideration of parameters generic to most bridges [7] has indicated that $\Delta\sigma_{p(cont)}$ is very small relative to $\Delta\sigma_p$ determined by analysis that ignores the time-dependent changes in these moments.

5. Development of design aids

The geometric coefficients k_A, k_I, k_{cc}, and k_p (Eq. (18)) depend upon the geometry of the section and the material parameters $E_f/E_c(t_0)$, $E_p/E_c(t_0)$, and $\chi\varphi$. The most common girder cross sections likely to be used with FRP tendons are single- or double-T (DT) girders. Therefore, in lieu of using Eq. (18), design aids for the geometric coefficients for a typical DT post-tensioned section (Fig. 3) are presented in Figs. 6 and 7 for sections with CFRP and AFRP tendons, respectively. In these figures, the ratio of FRP reinforcement in the flange is $\rho_f = A_f/(bh_f)$, and the ratio of prestressing steel area to area of webs is $\rho_p = A_p/(h\Sigma b_w)$. Linear interpolation can be used for ρ_f and ρ_p values not shown in the graphs.

It is noted that the following assumptions are made in Figs. 6 and 7: (1) the FRP reinforcement is located at mid-depth of the flange; Eq. (2) FRP reinforcement in the webs is ignored; Eq. (3) distance from section top fiber to centroid of prestressing tendons, $d_p = 0.8h$; Eq. (4) $\Sigma b_w/b = 0.2$; and Eq. (5) $h_f/h = 0.10$. For sections with CFRP tendons (Fig. 6), $E_f/E_c(t_0) = E_p/E_c(t_0) = 5.6$; whereas for sections with AFRP tendons (Fig. 7) $E_f/E_c(t_0) = E_p/E_c(t_0) = 2.6$. No graph is presented for k_p in Fig. 6 since relaxation is negligible for CFRP tendons.

6. Illustrative example

The pretensioned girder shown in Fig. 8(a) is subjected to its self-weight and a prestressing force P at transfer (after elastic losses) of 2640 kN. The example considers using CFRP, AFRP, or steel strands to provide the required prestressing force. In each case, the required area of prestressing strands is calculated and the proposed method is used to find the long-term prestress loss and the change in concrete strains and stresses for a section at mid-span. Long-term deflections at mid-span are then compared in the three cases. The flange of the DT section is assumed to have non-prestressed reinforcement of area = 1200 mm^2 (0.5%

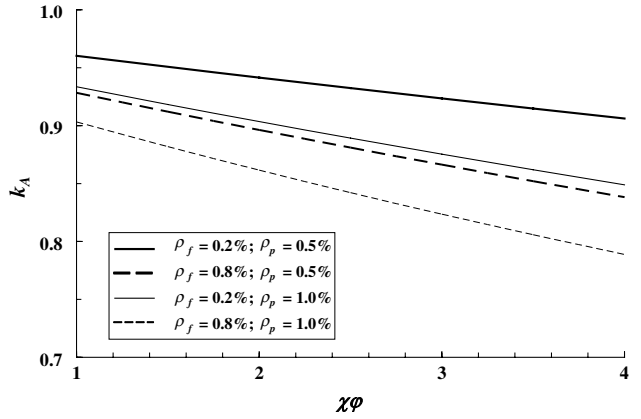

Fig. 6a. Geometry coefficient, k_A, for DT sections with CFRP tendons.

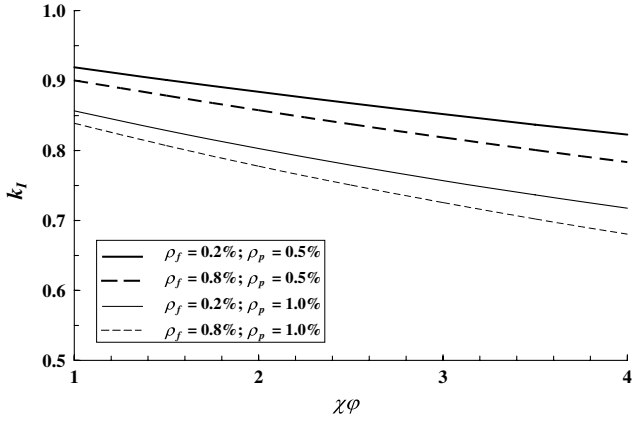

Fig. 6b. Geometry coefficient, k_I, for DT sections with CFRP tendons.

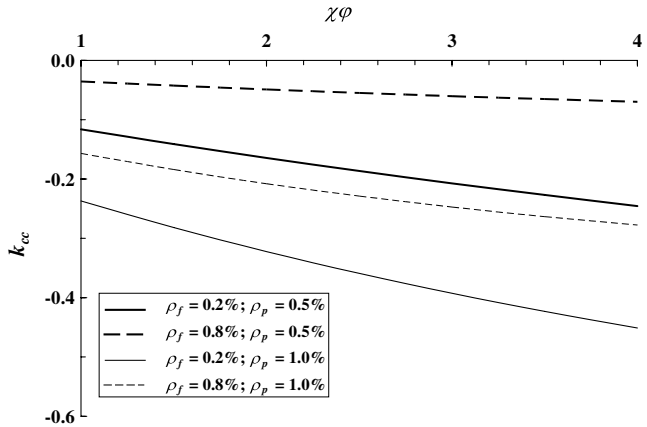

Fig. 6c. Geometry coefficient, k_{cc}, for DT sections with CFRP tendons.

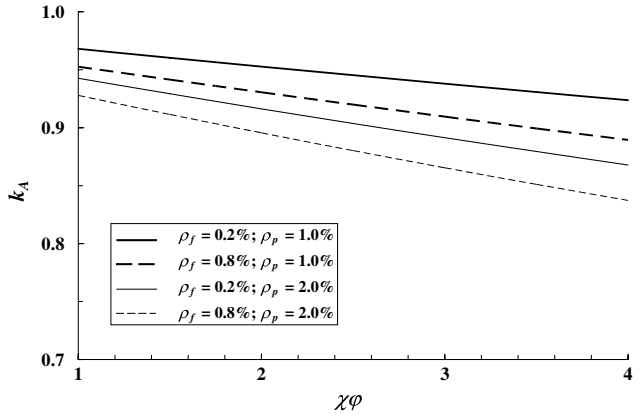

Fig. 7a. Geometry coefficient, k_A, for DT sections with AFRP tendons.

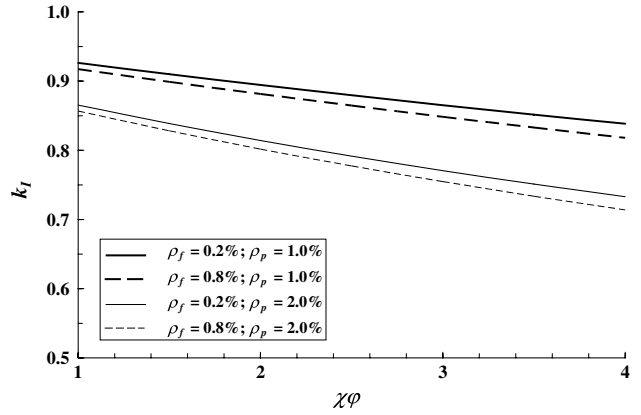

Fig. 7b. Geometry coefficient, k_I, for DT sections with AFRP tendons.

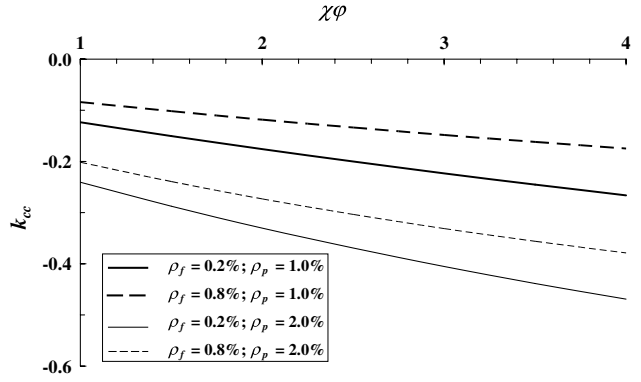

Fig. 7c. Geometry coefficient, k_{cc}, for DT sections with AFRP tendons.

A_f) of the same material used for prestressing strands. For long-term effects, it is assumed that $\varepsilon_{cs} = -400 \times 10^{-6}$, $\chi\varphi$ varies from 1 to 4, $E_c(t_0) = 25$ GPa, and $\chi = 0.8$. Other details of material properties are listed in Table 1, where α_{ps} and α_{ns} are the ratio of modulus of elasticity of prestressing and non-prestressed steel to $E_c(t_0)$, respectively.

The required areas of prestressing tendons of materials listed in Table 1 are determined using the allowable stresses for CFRP and AFRP according to ACI 440.4 [1] and the allowable values for steel according to AASHTO-LFRD

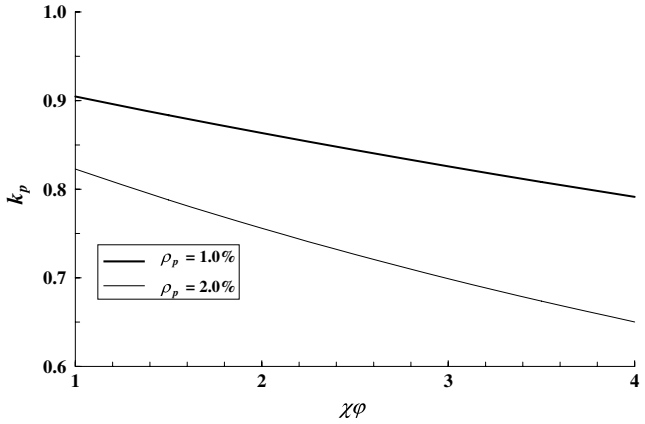

Fig. 7d. Geometry coefficient, k_p, for DT sections with AFRP tendons.

[8]. The reduced relaxation $\Delta\bar{\sigma}_{pr}$ for AFRP was calculated using Eq. (3), assuming $\chi_r = 0.95$. $\Delta\bar{\sigma}_{pr}$ for steel was calculated according to AASHTO-LFRD [8] for low-relaxation strands with $\chi_r = 0.7$.

Table 2 summarizes the analysis results using the proposed method for the case of $\chi\varphi = 2.0$. The changes in strains and stresses for the case of CFRP tendons with $\chi\varphi = 2.0$ are depicted in Fig. 8(b). The absolute values of long-term prestress losses, $\Delta\sigma_p$, are compared in Fig. 9. In each case, $\Delta\sigma_p$ was calculated using Eq. (21) with the coefficients k_A, k_I, k_{cc}, and k_p obtained by interpolation from Figs. 6 and 7. It should be noted that an increase in $\chi\varphi$ essentially represents an increase in the creep coefficient φ since χ is assumed to have a constant value of 0.8. As expected, $\Delta\sigma_p$ increases with the increase in $\chi\varphi$, with the case of using steel strands being the largest, followed by CFRP then AFRP. This is mainly because of the difference in their respective moduli of elasticity. For instance at $\chi\varphi = 2.0$, the ratio of $\Delta\sigma_p$ for CFRP to that of steel is 0.69 (see Table 2), which is almost equal to the ratio of their respective moduli of elasticity $E_f(\text{CFRP}))/E_s = 0.7$. However, this is not the case when comparing $\Delta\sigma_p$ for CFRP and AFRP where the ratio of $\Delta\sigma_p$ for AFRP to that of CFRP is 0.75, whereas $E_f(\text{AFRP})/E_f(\text{CFRP}) = 0.46$. This is because of the additional prestress loss due to relaxation in AFRP strands. It is thus seen that, applying the same empirical equations used to predict prestress loss in steel strands to FRP strands cannot yield accurate or even reasonable results in all cases.

The coefficient Ω (Eq. (6)) for the case of AFRP tendons varies from 0.1 to 0.2 as $\chi\varphi$ increases from 1 to 4. From Fig. 1 with $\lambda = 0.4$, it can be found that χ_r varies from 0.97 to 0.94; therefore, the assumption of $\chi_r = 0.95$ made earlier would appear to be reasonable.

The residual compression stress in concrete after an extended period of time at critical locations (bottom fibers for sections at mid-span and top fibers for sections at support) is of particular importance since these are the locations that are most susceptible to cracking under additional live load. Eq. (22) is used to estimate the change in concrete stress at the extreme bottom fiber in a section at mid-span.

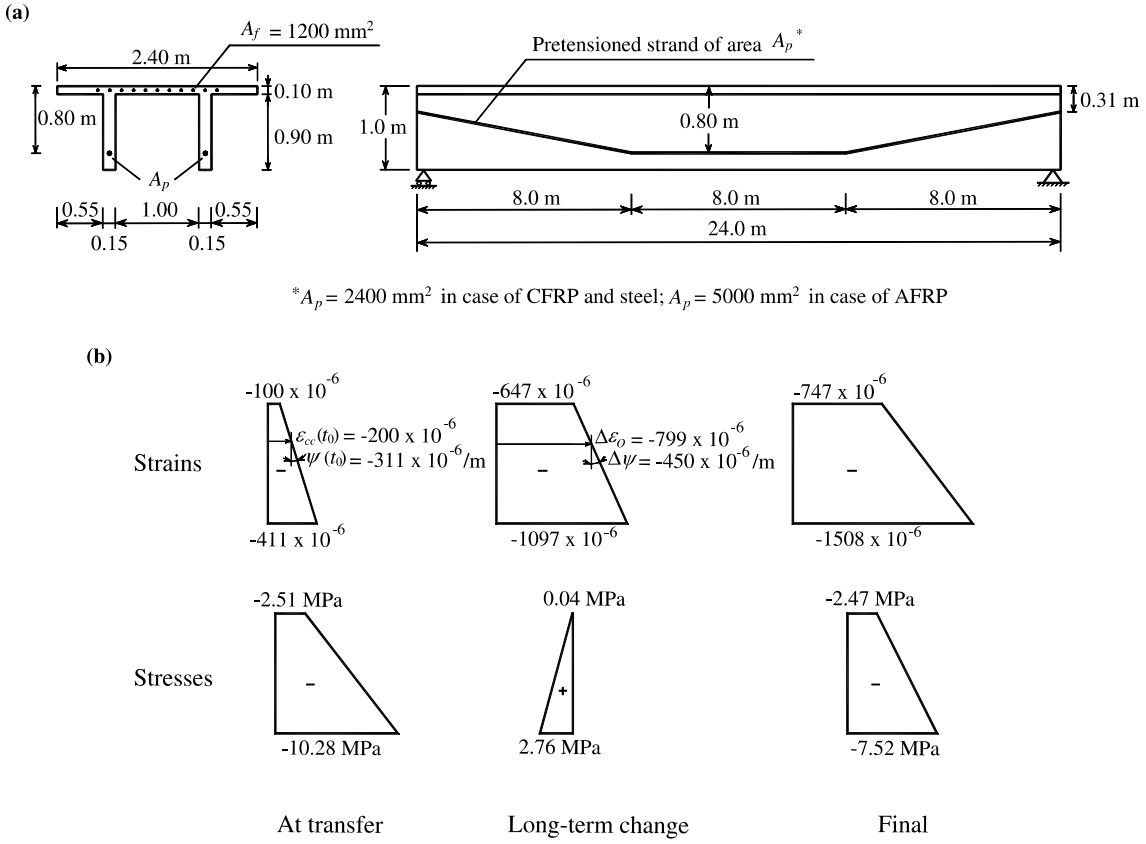

Fig. 8. Pretensioned girder analyzed in the example (a) Geometric dimensions and (b) strains and stresses at transfer and final for the case of using CFRP tendons and $\chi\varphi = 2.0$.

Table 1
Properties of CFRP, AFRP, and steel prestressing tendons considered in the illustrative examples

	$\alpha_p = \alpha_f$ or $\alpha_{ps} = \alpha_{ns}$	f_{pu} (MPa)	Allowable stress after transfer	A_p or A_{ps} (mm²)	σ_{p0} (MPa)	$\Delta\bar{\sigma}_{pr}$ (MPa)
CFRP	5.6	2000	$0.6f_{pu}$	2400	1100	0
AFRP	2.8	1200	$0.40f_{pu}$	5000	528	−25
Steel	8.0	1860	$0.7f_{pu}$	2400	1100	−50

This change in concrete stress is added to the initial stress at transfer to give the final concrete stress $\sigma_{bot(final)}$ after an extended period of time, which is shown in Fig. 10. The immediate stresses are slightly different because of the variance in the moduli of elasticity of each material and in the area of prestressing strands (in case of AFRP tendons). The absolute value of the residual concrete compression decreases with the increase of creep values. The decrease in compression was the smallest and the greatest in the cases of CFRP tendons and AFRP tendons, respectively.

Table 2
Analysis results for the case of $\chi\varphi = 2$

	CFRP	AFRP	Steel
$\sigma_{top}(t_0)$ (MPa)	−2.51	−2.54	−2.47
$\sigma_{bot}(t_0)$ (MPa)	−10.28	−10.45	−10.03
$\Delta\varepsilon_O$	-7.988×10^{-4}	-7.665×10^{-4}	-7.429×10^{-4}
$\Delta\psi$(/mm)	-4.497×10^{-7}	-1.926×10^{-7}	-3.356×10^{-7}
$\Delta\sigma_{top}$ (MPa)	0.036	−0.39	0.17
$\Delta\sigma_{bot}$ (MPa)	2.76	4.60	3.68
$\sigma_{bot(final)}$ (MPa)	−2.47	−2.93	−2.30
$\sigma_{top(final)}$ (MPa)	−7.52	−5.85	−6.35
$\Delta\sigma_{ps}$ (MPa)	−140.9	−105.6	−203.5
ΔD (mm)	−26.98	−11.56	−20.14

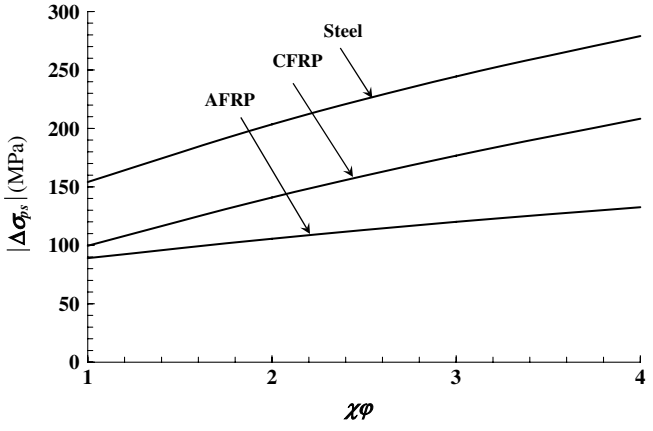

Fig. 9. Effect of creep on long-term prestress loss in concrete girder with CFRP, AFRP or steel tendons.

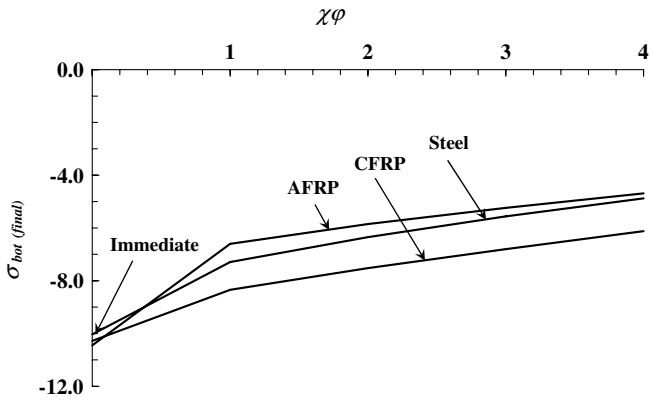

Fig. 10. Effect of creep on the residual concrete stress at the extreme bottom fiber of prestressed concrete girder with CFRP, AFRP or steel tendons.

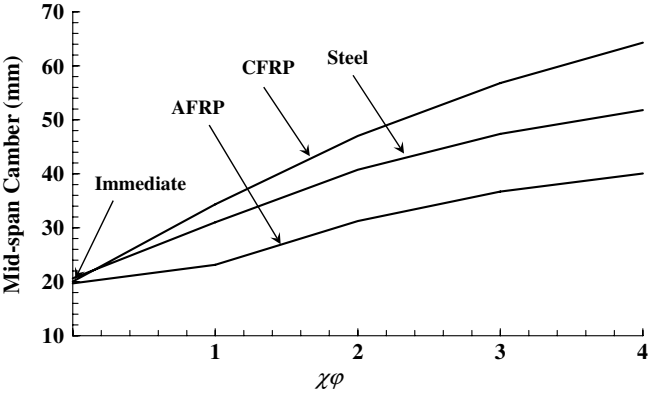

Fig. 11. Effect of creep on the long-term camber at mid-span of a concrete girder with CFRP, AFRP or steel tendons.

The long-term change in curvature $\Delta\psi$ is used to calculate the long-term deflection ΔD (Eq. (23)) and the total absolute deflection (immediate plus long-term) at mid-span is plotted in Fig. 11 for the three cases. The immediate deflection was about 20 mm upward (camber) for the three cases. The girder prestressed with CFRP showed the largest increase in camber with time, followed by steel and AFRP. This is because of the relaxation effects in steel and AFRP tendons, which tend to produce downward deflection in simply supported girders. Had the initial deflection been downward (the downward deflection due to dead load is larger than the upward deflection due to prestressing), the girder with AFRP tendons would have displayed the largest increase in downward deflection. Again, this clearly shows that adopting empirical multipliers as recommended by current codes of practice to estimate the long-term increase in deflection does not produce reliable results in all cases.

7. Summary

A simple method is presented to estimate the long-term prestress loss in continuous concrete girders with FRP tendons as well as the time-dependent change in concrete stresses and deflections at critical sections assuming uncracked conditions. The method presented can be easily programmed using hand-held calculators or computer spread sheets. A simple graphical tool is proposed to calculate the reduced relaxation coefficient χ_r for AFRP tendons to be used in applying the method to prestressed girders with AFRP tendons and a value of $\chi_r = 0.95$ is suggested for practical purposes. For the most common DT prestressed girders used in practice, design aids are presented to further simplify the method for practicing engineers.

The long-term prestress loss in concrete girders prestressed with FRP tendons is less than that when using steel tendons, mainly because of the lower moduli of elasticity of FRP. The time-dependent change in concrete stresses and deflection can be either smaller or greater than those of comparable girders prestressed with steel tendons, depending on the type of FRP tendons and the initial stress profile (due to dead load and prestressing) of the prestressed cross-section at member mid-span.

Acknowledgements

The authors gratefully acknowledge the financial support provided by California Department of Transportation under Research Grant No. 59A0420.

References

[1] ACI Committee 440.4R-04 Prestressing concrete structures with FRP tendons. American Concrete Institute. Farmington Hills, MI, 2004.
[2] Saadatmanesh H, Tannous FE. Long-term behavior of aramid fiber reinforced plastic (AFRP) tendons. ACI Mater J 1999;96(3): 297–305.
[3] Ghali A, Trevino J. Relaxation of steel in prestressed concrete. PCI J 1985;30(5):82–94.
[4] Ghali A, Favre R, Elbadry MM. Concrete Structures, Stresses and Deformations. 3rd ed. London & New York: Spon Press; 2002.
[5] Trost H. Auswirkungen des Superpositionsprinzips auf Kriech-und Relaxations-problems bei Beton und Spannbeton. Beton Stahlbetonbaun 1967;62(10):230–8 (62)11: 261–269 (in German).
[6] Bazant ZP. Prediction of concrete creep effects using age-adjusted effective modulus. ACI J 1972;69(4):212–7.
[7] Youakim SA, Karbhari VM. A Simplified method for prediction of long-term prestress loss in post-tensioned concrete bridges. Caltrans Draft Report. University of California at San Diego, CA, 2004.
[8] American Association of State Highway and Transportation Officials AASHTO-LRFD bridge design specifications. 3rd ed., Washington DC, 2004.